Letters on Materials 15 (4), 2025 pp. 376-382 www.lettersonmaterials.com

Received 26 September 2025; Accepted 19 November 2025
https://doi.org/10.48612/letters/2025-4-376-382 https://elibrary.ru/fwbovu

Effect of heat treatment on the microstructure and properties of solid-state joints of dissimilar Ni-based superalloys

E. V. Galieva[†1], A. A. Tagirova[1], R. R. Gabbasov[1], V. A. Valitov[1,2]

[†]galieva_elvina_v@mail.ru

[1]Institute for Metals Superplasticity Problems, Russian Academy of Sciences, Ufa 450001, Russia
[2]Ufa University of Science and Technology, Ufa 450076, Russia

Abstract: This article discusses the effects of solid-state bonding (SSB) and subsequent heat treatment (HT) on the microstructure, phase composition, and mechanical properties of solid-state joints (SSJ) made of wrought (EK61) and powder (EP741NP) heat-resistant nickel superalloys. SSB was performed in a vacuum under the temperature gradually increasing from 850°C to 1000°C. After SSB, in the EK61 superalloy transformation of the ultrafine-grained structure into a coarse-grained one with an average grain size of 38 ± 7 μm is observed, while the microstructure of the EP741NP superalloy remained of fine-grained microduplex type. After subsequent HT, grain growth is observed up to the size of 300 ± 48 μm in the EK61 superalloy and up to 49 ± 5 μm in the EP741NP superalloy. The width of the diffusion zone after SSB was 18 μm, and after HT it increased significantly, up to 150 μm. The results of mechanical tests showed that the fracture of the obtained EK61//EP741NP joints immediately after SSB occurred in the SSJ zone, and after subsequent HT, the fracture occurred outside the SSJ zone in the less heat-resistant EK61 superalloy. The strength after SSB is 660 MPa, and after following HT it is 770 MPa. It was found that after SSB, the microhardness of the EK61 superalloy decreased from 3.9 GPa to 2.4 GPa, and in the EP741NP superalloy it remained at the level of the initial state. In the SSJ zone, the microhardness, both after SSB and after HT, possesses intermediate values between the microhardness values of the superalloys being joined.

Keywords: nickel superalloys, microstructure, strength, solid-state bonding, solid-state joint, heat treatment

Acknowledgement: *The work was supported by the State assignment of the Institute for Metals Superplasticity Problems of the Russian Academy of Sciences No. 124022900007-9. Experiments, microstructural studies and mechanical tests were performed in the center of collective use of the Institute for Metals Superplasticity Problems of the Russian Academy of Sciences.*

1. Introduction

Currently, the aircraft engine building and power engineering industry face the challenge of creating reliable permanent joints of heat-resistant nickel superalloys that are used under conditions of high temperature gradients and significant mechanical loads [1–4]. The development of effective bonding technologies allows for high strength and durability of structures. Examples of such promising structures are bimetallic structures of the "blisk" type (one-piece joint of a disk with blades) and "disk-shaft" [2, 5–7]. However, the processing and production of high-quality SSJ from hard-to-deform high-alloy heat-resistant nickel superalloys are associated with a number of technological difficulties due to their specific physical, chemical and mechanical properties [1–3, 2–8].

The solution to the above problem will expand the areas of application of bimetallic parts of gas turbine engines (GTEs). This will significantly reduce the weight of prospective GTEs and improve their energy efficiency and performance characteristics, in particular, by increasing their durability under cyclic thermomechanical effects [9–12]. This is especially important when using modern heat-resistant nickel superalloys, which are characterized by high heat resistance and corrosion resistance [13–16].

However, to implement this task, it is necessary to develop scientific and technical proposals for obtaining high-strength one-piece joints, for example, between wrought and powder heat-resistant nickel superalloys. Traditional methods of fusion welding, including arc welding in a protective gas environment, spark plasma sintering, electron beam and laser bonding, make it possible to obtain strong joints [17–23]. It should be noted that bonding of high-alloy heat-resistant nickel superalloys using the specified methods is often accompanied by the formation of defects such as thermal cracks, porosity, heterogeneity of the microstructure and phase composition in the joint zone, which can significantly reduce the performance characteristics of bonded joints [24–26].

Today, the promising methods for obtaining solid-state joints are diffusion bonding, types of friction welding (linear friction welding, rotary friction welding and friction stir welding) or spark plasma sintering [27–36]. Diffusion bonding is an effective alternative to traditional methods of joining heat-resistant nickel superalloys [27, 28]. The diffusion bonding process involves plastic creep deformation [28], usually within 5%. However, diffusion bonding is carried out mainly at high temperatures, exceeding the temperature of complete dissolution of the strengthening phase. Therefore, after diffusion bonding, a significant coarsening of the original microstructure can be observed, which can lead to a decrease in the strength characteristics of the heat-resistant superalloy by 10–15%. Despite the effectiveness of friction welding, it has a number of disadvantages, such as the formation of a heat-affected zone in which a heterogeneous structure is formed, high probability of residual stresses, and limited applicability for complex-shaped parts [29–31]. All the above mentioned disadvantages can be eliminated by using the solid-state bonding (SSB) method using superplastic deformation [31,32,37,38]. This method ensures the formation of a homogeneous structure in the solid-state joint (SSJ) zone without a temperature gradient, which allows achieving strength characteristics at the level of the base material. In addition, reducing the welding temperature by 200°C or more compared to temperatures in traditional diffusion bonding allows reducing energy costs and the thermal impact on the material, while maintaining its original properties [32,38].

To ensure high performance characteristics of superalloys, it is necessary, among other things, to apply heat treatment (HT) after SSB, aimed at eliminating residual stresses, increasing thermal stability and ensuring uniformity of the microstructure, as well as homogeneous precipitation of intragranular coherent particles of the strengthening phase [1–3,39–43].

The aim of the study is to establish the effect of HT on the change in the microstructure, phase composition and properties of solid-state joints made from heat-resistant nickel superalloys EK61 (wrought) and EP741NP (powder), which differ not only in chemical composition and type of strengthening phase, but also in the method of their production.

2. Materials and methods

2.1. Materials

The materials under study were the wrought EK61 superalloy and powder EP741NP superalloy obtained by powder metallurgy. The chemical composition of the materials under study is given in Table 1. The chemical composition of the superalloy EK61 corresponds to TU 14-1-50-45-91, and EP741NP corresponds to GOST R 52802-2007.

The wrought EK61 superalloy has an ultrafine-grained microstructure of a mixed type, formed as a result of preliminary deformation and heat treatment in the temperature range of 950–850°C. The average size of the γ-phase grains and incoherent δ-phase particles is 0.3–0.8 μm, the volume fraction of the δ-phase is 24%. In addition to ultrafine grains, relatively large δ-phase particles (up to 2 μm in size) are observed in the microstructure, the fraction of which is 5% [32]. Powder superalloy EP741NP has a fine-grained microstructure of the microduplex type, obtained according to the modes given in the [44]. The microduplex structure is represented by grains of the matrix γ-phase in the EP741NP superalloy with an average size of 5.5 ± 0.6 μm. Along the boundaries and in triple junctions of γ-phase grains, there are incoherent precipitates of the γ'-phase based on the intermetallic compound $Ni_3(Al,Ti)$ with a size of 2.9 ± 0.7 μm. In addition, coherent dispersed particles of the γ'-phase are uniformly precipitated inside the γ-phase grains, which are usually formed during cooling to room temperature after high-temperature deformation treatment, or during the aging process of final HT.

2.2. Methods

Solid-state bonding. Experiments on SSB in vacuum were carried out using specimens in a combination of EK61//EP741NP superalloys with a step-by-step increase in temperature: 850°C → 900°C → 950°C → 1000°C. Bonding was carried out using an original UVSD-1 device for high-temperature (up to 1250°C) SSB, including a high-temperature furnace, strikers made of intermetallic superalloy type VKNA, a cooling system for the load cell of the Schenck Trebel testing machine type RMS100 and equipment (forevacuum + diffusion pumps) for creating a vacuum during the deformation treatment of the materials being joined. The vacuum depth was $P = 5 \cdot 10^{-2}$ Pa. The SSB experiments were conducted using cylindrical specimens with the same diameter of 16 mm with the following height values of 20 and 16 mm for EK61 and EP741NP superalloys, respectively. The prepared specimens were placed in a sealed stainless steel container. Vacuum was created and maintained inside the container along with the specimens during the entire SSB process. The deformation of the specimens together with the container was carried out according to the uniaxial compression scheme on a Schenck Trebel RMS100 testing machine. During the SSB, the container's tightness was not violated.

Heat treatment. After SSB, some of the deformed specimens in the EK61//EP741NP superalloy combination were subjected to HT, including high-temperature annealing at 1200°C and subsequent aging at 950°C in an ATS electric furnace. The heat treatment temperature conditions were chosen to be suitable for the more heat-resistant EP741NP superalloy.

Microstructure analysis. Microstructural studies were performed using a Mira 3LMH scanning electron microscope. Electropolished specimens were used for microstructural studies using the EBSD analysis method. The scanning step for EBSD analysis was 0.3–0.8 μm using the CHANNEL 5 program. The distribution of elements was studied using the energy-dispersive analysis method using a Tescan VEGA 3SBH scanning electron microscope with an EDX attachment.

Table 1. The chemical composition of nickel superalloys (the main alloying elements, %).

Superalloy	Al	Cr	Co	W/V	Fe	Mo	Ti	Nb	Cu	C	Ni
EK61	1.0	16.6	-	0.5V	15.0	3.9	0.8	5.0	0.5	≤0.05	Base
EP741NP	5.0	9.0	15.7	5.6W	≤0.5	3.8	1.8	2.6	-	0.035	

Mechanical testing. Mechanical tests were carried out at room temperature on flat specimens with a working section of 3 mm × 2 mm and a working length of 6 mm, cut from the central part of welded blanks. The travel speed was 0.5 mm/min.

Microhardness measurement. Microhardness was measured using a MNT-10 microhardness tester. The load was 100 g, the loading rate was 50 g/s, and the holding time was 10 s. Microhardness was measured both in the base material and in the SSJ zone. Microhardness measurements were performed in accordance with GOST 9450-76.

3. Results

Figure 1 shows the microstructure in the SSJ zone and 2 mm away from the SSJ after the SSB (Fig. 1a, c, e) and subsequent HT (Fig. 1b, d, f) of EK61//EP741NP superalloys.

According to the microstructural analysis, it was established that after the SSB, the EP741NP superalloy retained its initial fine-grained microduplex-type microstructure. However, in the EK61 superalloy, after SSB with a step-by-step increase in temperature from 850 to 1000°C, the ultrafine-grained microstructure was transformed into a coarse-grained one with an average grain size of the matrix phase of 38 ± 7 μm. The porosity after SSB was 12%.

After HT in the bonding specimen EK61//EP741NP there is a significant grain growth in both superalloys: in the EK61 superalloy the grain size is 300 ± 48 μm, in the EP741NP superalloy it is 49±5 μm. The porosity decreased and was about 5%.

Figure 2 shows the EBSD maps of the microstructure in the SSJ zone after SSB (Fig. 2 a) and subsequent HT (Fig. 2 b).

Figure 3 shows graphs of dependences of the concentration of diffusing elements on distance from the SSJ of EK61//EP741NP. The dotted lines indicate the boundaries of the diffusion interaction region (diffusion zone) of the superalloys being joined. In the combination of EK61//EP741NP superalloys, active diffusion of Co, W and Al from the EP741NP powder superalloy into the deformed EK61 superalloy and counter diffusion of Cr, Fe and Nb occurs. The width of the diffusion zone after SSB was 18 μm, and after HT the width of the diffusion zone increased significantly, up to 150 μm (more than 8 times). It should be noted that within the diffusion zone after HT, a more monotonous change in the chemical composition is observed upon transition from one joined superalloy to the other; brittle particles of intermetallic phases are not detected.

Table 2 shows the results of mechanical tests at room temperature for tension of flat specimens cut from EK61//EP741NP bonded samples. It was found that immediately after SSB, failure occurs in the SSJ zone, while in the case of SSB and subsequent HT, it occurs outside the SSJ zone in the less heat-resistant EK61 superalloy. It is shown, that the strength of EK61//EP741NP after SSB is 660 MPa that is 0.4 of the strength of EK61 with ultrafine-grained microstructure. And following HT increases its level up to 0.5 one.

The results of fractographic analysis of the fracture surfaces of bonded specimens EK61//EP741NP after both SSB and subsequent HT are shown in Fig. 4.

The fracture surface has both dimples and chips. Also, on both halves there are visible signs of seizing and cracks. The

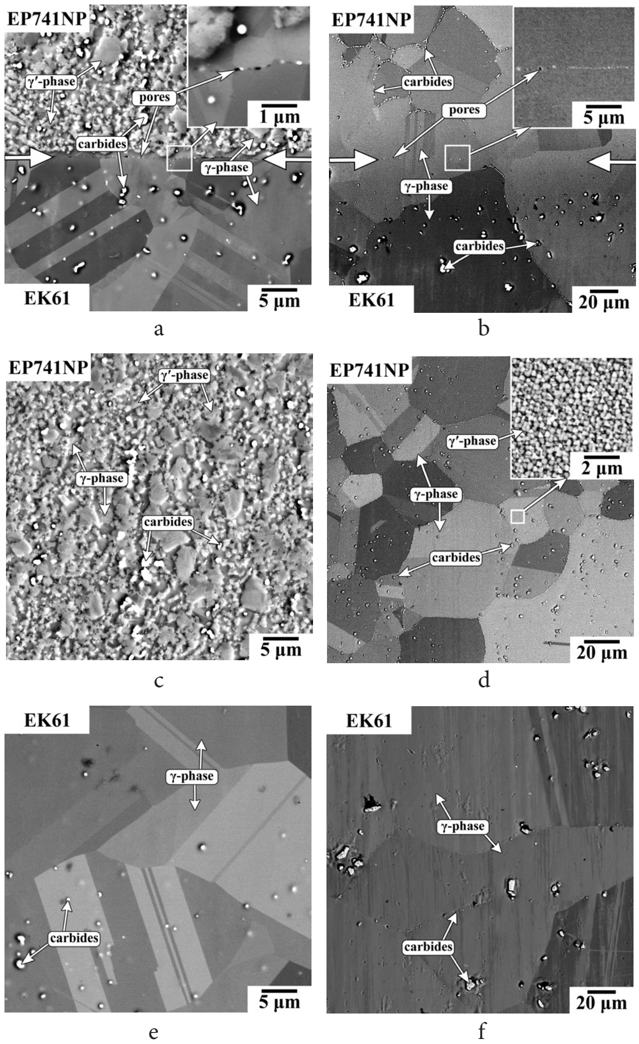

Fig. 1. The microstructure of SSJ (a, b) and in the depht of 2 mm of EP741NP (c, d) and EK61 (e, f) superalloys after SSB (solid-state bonding) (a, c, e) and SSB + HT (solid-state bonding and following heat treatment) (b, d, f).

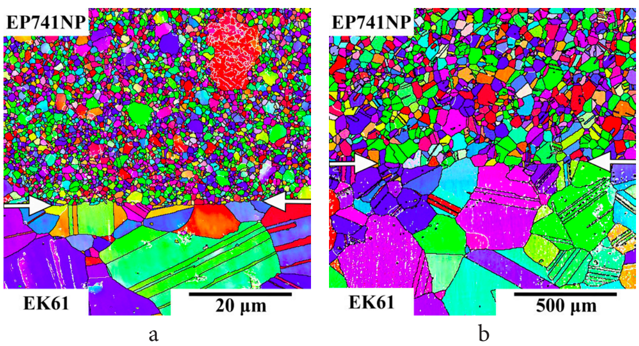

Fig. 2. (Color online) The EBSD maps of the SSJ zone of EK61//EP741NP after solid-state bonding (a) and following heat treatment (b).

fracture surface of the bonded specimens has a pronounced relief (Fig. 5). On the side of the EP741NP superalloy, slip lines are visible in the grains of the matrix phase, and this pattern is observed in large grains. The area in which such grains are present is 500 – 700 μm from the interface between the two superalloys, and at further distances the grains are not deformed. In the EK61 superalloy, slip planes are also visible throughout the material.

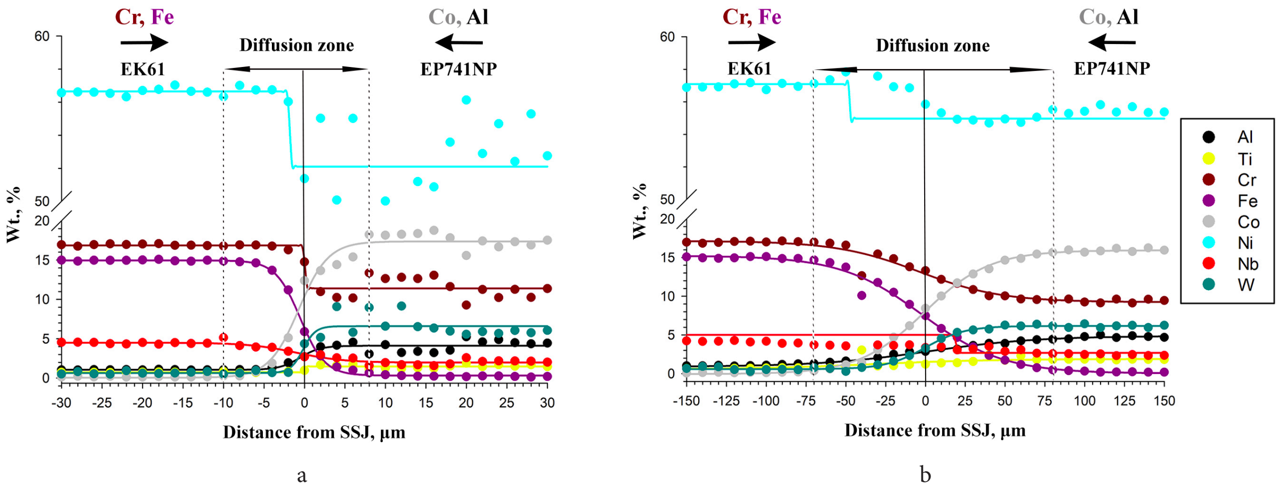

Fig. 3. (Color online) The distribution of alloying elements in the solid-state joint of EK61//sEP741NP after solid-state bonding (a) and heat treatment (b).

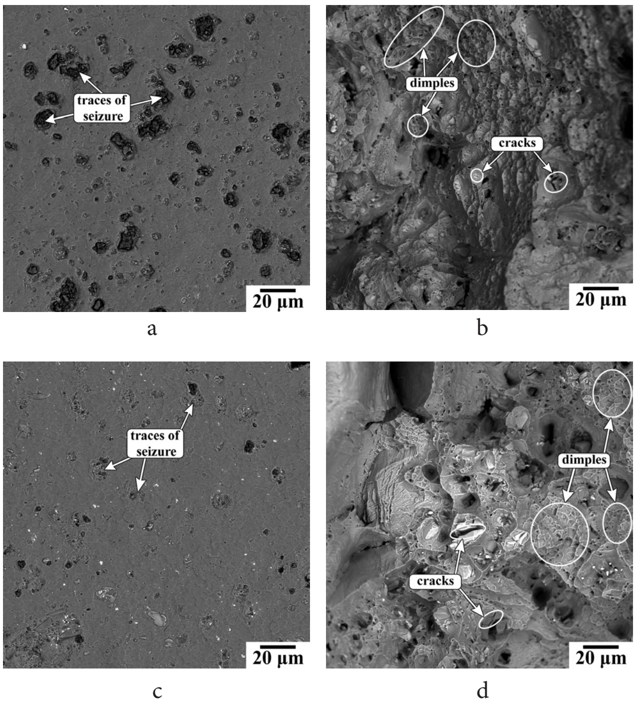

Fig. 4. The fracture surfaces of bonded specimens after SSB (a, c) and SSB + HT (b, d): one piece of bonded specimens (a, b); another piece of bonded specimens (c, d).

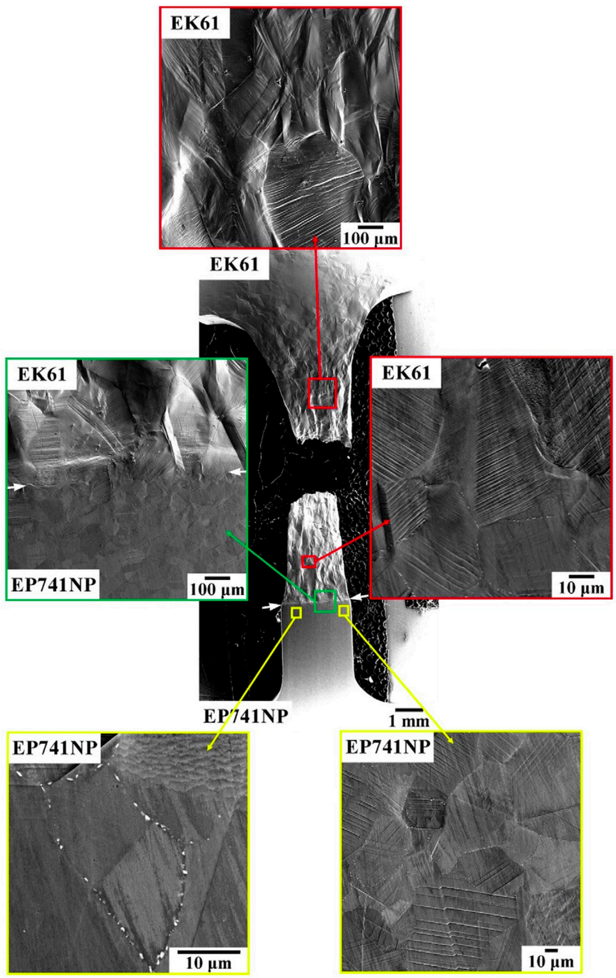

Fig. 5. (Color online) Surface relief of bonded EK61//EP741NP specimens after mechanical tensile testing at 20°C (SSB + HT).

Table 2. The strength of EK61//EP741NP after SSB and following HT at room temperature.

Specimen	Condition	σ_B, MPa
EK61//EP741NP	SSB	660 ± 85
	SSB + HT	770 ± 85

Table 3 shows the results of microhardness measurements both in the area of the base materials and in the solid-state joint zones. According to the results of microhardness measurements, it was found that after SSB the microhardness of the EK61 superalloy decreased from 3.9 GPa to 2.4 GPa, and in the EP741NP superalloy it remained at the level of the initial state. In the SSJ zone, the microhardness, both after SSB and after HT, occupies intermediate values between the microhardness values of the superalloys being joined.

Table 3. The microhadneess of EK61//EP741NP after SSB and following HT at room temperature.

Specimen	Condition	Microhadneess, GPa		
		EK61	In the SSJ	EP741NP
Initial state	–	3.9 ± 0.2	–	5.6 ± 0.2
EK61//EP741NP	SSB	2.4 ± 0.4	3.6 ± 0.3	5.4 ± 0.2
	SSB+HT	3.1 ± 0.3	4.6 ± 0.3	5.2 ± 0.2

4. Discussion

In the presented work, bonded joints of EK61 and EP741NP superalloys were successfully obtained by SSB with a step-by-step increase in temperature in following stages 850°C→900°C→950°C→1000°C. The choice of such temperature conditions of SSB in the combination of EK61//EP741NP superalloys was due to the fact that in this case superplasticity will manifest itself both in the EK61 superalloy and in the EP741NP superalloy. Forming solid-state joint is occurred both by superplastic deformation and by diffusion of alloying elements.

Figure 6 presents distribution maps of alloying elements at the interface region obtained in SE mode. At the right part of the figure, higher magnification maps are given for the small area highlighted by the red square.

Particles enriched in carbide-forming elements such as Mo, Nb, and Ti and depleted in Cr are visible in SE images and maps of alloying element distribution (Fig. 6). These particles are located both along the grain boundaries of the matrix phase and within the grains. During heat treatment, diffusion within the bulk of the material prevails over diffusion along the grain boundaries. This is evidenced by the intermediate composition of the matrix phase grain interior. For instance, after heat treatment, the grains of the EK61 superalloy adjacent to the interface between the two alloys have an intermediate chemical composition. This results in the different phase composition within a single matrix γ-grain. The γ'-phase precipitates are observed in the matrix grains of the gamma phase, which presented Fig. 6b in red square. Such precipitates are revealed to a depth of about 50 μm toward the EK61 superalloy (noted in Fig. 6b by yellow line and arrows).

Both γ-grains adjacent to the interface of EK61 and SSJ zone have an intermediate chemical composition between the ones of the superalloys joined. Any brittle particles are not visible, that is confirmed by the absence of peaks in the microhardness values indicated. In addition, the distribution maps of alloying elements show that the joint interface is sharp in the specimens after SSB, while after HT it is blurred.

Thus, the HT led to significant changes in the microstructure and phase composition in the solid-state joint zone of EK61//EP741NP superalloys and far from this zone. The microstructure of both superalloys became coarse-grained, and the visible line of the solid-phase bond became more sinuous. Noted change is likely due to migration of grain boundaries. As well as, during HT, in the process of collective recrystallization in the SSJ zone of EK61 and EP741NP superalloys, common grains are formed. At the same time, the change in the content of alloying elements when moving from one joined superalloy to the other became smoother. However, according to the microstructural and mechanical testing results noted above, it should be noted, that selected heat treatment conditions are not optimal, since they led to excessive grain growth to 300±48 μm in the EK61 superalloy. With such a large grain size, the tensile strength of the EK61 superalloy is 15–20% lower than in the material with a smaller grain size (30–40 μm). Despite the fact that fracture occurred along the EK61 superalloy, the tensile strength level

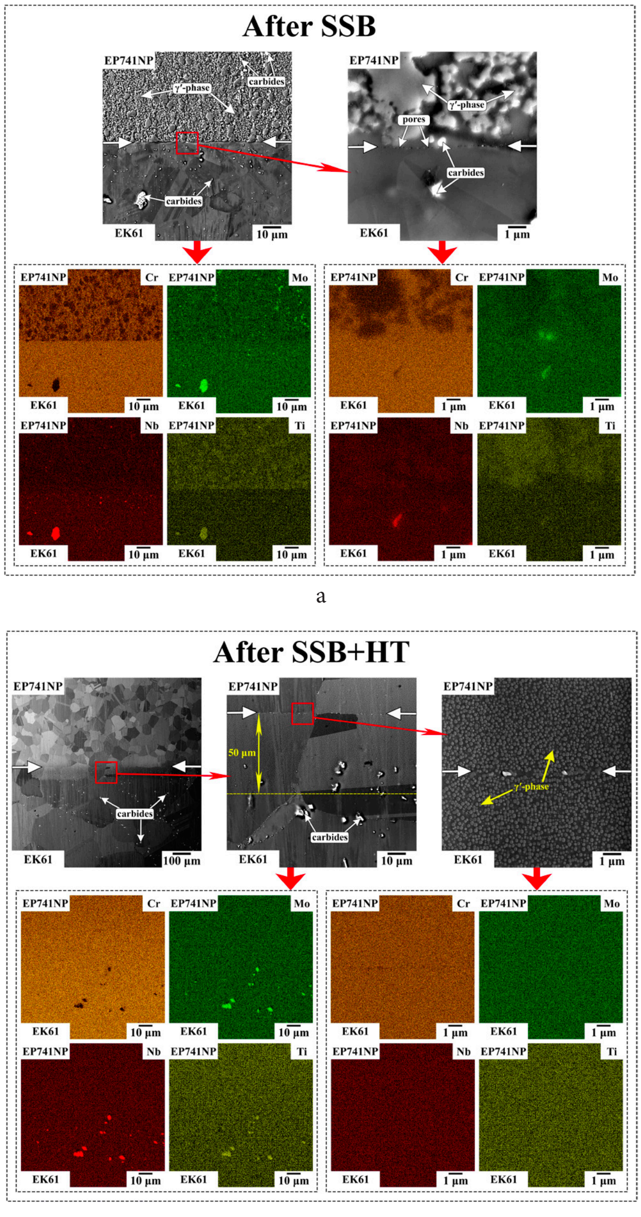

Fig. 6. (Color online) Microstructure and maps of alloying element distribution (Cr, Mo, Nb, Ti) in the SSJ zone after SSB (a) and SSB+HT (b).

is 0.5 of the tensile strength of the EK61 superalloy with the original UFG microstructure. After fracture of the welded specimens, signs of bonding are observed. The fracture most likely occurred along the grain boundaries of the EP741NP superalloy. In the heat-treated specimens, crack initiation during fracture occurred in the matrix phase grains of the EK61 superalloy. Cracks are observed on flat surfaces corresponding to the cleavage planes. The presence of both cleavage zones and pits suggests a mixed fracture pattern.

5. Conclusion

The solid-state bonding method in temperature range 850–1000°C allowed for obtaining SSJ of heat-resistant EK61 and EP741NP nickel superalloys. After heat treatment of EK61// EP741NP bonded samples the microstructure of both superalloys became coarse-grained one with grains of the γ-matrix phase 300 ± 48 μm in EK61 and 49 ± 5 μm in EP741NP superalloys.

After heat treatment, the γ-matrix phase grains in the heat-resistant EK61 superalloy adjacent to the interface between the two alloys have an intermediate chemical and phase composition. In the side of EK61 superalloy, γ'-phase precipitates are observed only within one matrix grain in a depth of about 50 μm.

The bonded specimens subjected to heat treatment failed outside the solid-state joint zone. However, heat treatment conditions used in the present study led to strong softening of the EK61 superalloy. The strength after SSB is 660 MPa, after subsequent heat treatment it is 770 MPa.

References

1. A. V. Logunov, Heat-resistant nickel alloys for gas turbine blades and discs, Gazoturbinnye Tekhnologii Publishing House, Rybinsk, 2017.
2. R. C. Reed, The superalloys: fundamentals and applications, Cambridge University Press, 2006.
3. B. S. Lomberg, S. V. Ovsepyan, M. M. Bakradze, M. N. Letnikov, I. S. Mazalov, The application of new wrought nickel alloys for advanced gas turbine engines, Aviat. Mater. Technol. (S) (2017) 116 – 129.
4. G. Gudivada, A. K. Pandey, Recent developments in nickel-based superalloys for gas turbine applications: Review, J. Alloys Compd. 963 (2023) 171128.
5. L. A. Magerramova, Application of bimetallic blisks manufatured by hip from powder and cast Ni-base superalloys for gas turbine lifeincrease, Vestnik UGATU. 15 (4 (44)) (2011) 33 – 38.
6. A. Mateo, On the feasibility of BLISK produced by linear friction welding, Rev. Metal. 50 (3) (2014) e023.
7. Q. Fan, High-Temperature alloys in aerospace applications and future innovations, Highl. Sci. Eng. Technol. 125 (2025) 296 – 302.
8. E. I. Razuvaev, M. V. Bubnov, M. M. Bakradze, S. A. Sidorov, Hot isostatic pressing and deformation of the granulated heat resistant nickel alloys, Aviat. Mater. Technol. (S1 (43)) (2016) 80 – 86.
9. A. Aublet, M. Rambaudon, F. N'Guyen, D. Ryckelynck, C. Remacha, R. Cariou, H. Proudhon, Mechanical fatigue testing under thermal gradient and manufacturing variabilities in nickel-based superalloy parts with air-cooling holes, Exp. Mech. 62 (7) (2022) 1079 – 1091.
10. J. Cao, F Jing., J. Yang, Thermal-mechanical fatigue behavior and life assessment of single crystal nickel-based superalloy, Crystals. 13 (5) (2023) 780.
11. A. Schmiedel, C. Burkhardt, S. Henkel, A. Weidner, H. Biermann, Very high cycle fatigue investigations on the fatigue strength of additive manufactured and conventionally wrought Inconel 718 at 873 K, Metals 11 (11) (2021) 1682.
12. M. Böcker, H. R. Babu, S. Henkel, M. Raddatz, U. Gampe, H. Biermann, Planar-biaxial thermo-mechanical fatigue behavior of nickel-base superalloy inconel 718 under proportional loading, Metall. Mater. Trans. A. 54 (5) (2023) 1971 – 1984.
13. S. M. Schackert, C. Schweizer, Investigation of damage mechanisms and short fatigue crack growth during thermomechanical fatigue loading of the nickel-based superalloy Inconel 100, Fatigue Fract. Eng. Mater. Struct. 45 (8) (2022) 2261 – 2276.
14. S. Guo, D. Xu, Y. Liang, Y. Li, J. Yang, G. Chen, D. D. Macdonald, Corrosion characteristics of typical Ni-Cr alloys and Ni-Cr-Mo alloys in supercritical water: a review, Ind. Eng. Chem. Res. 59 (42) (2020) 18727 – 18739.
15. S. Madhusudan, E. Epifano, J. Favergeon, T. Sanviemvongsak, D. Maréchal, D. Monceau, High temperature intergranular oxidation of nickel based superalloy inconel 718, High Temp. Corros. Mater. 101 (5) (2024) 873 – 884.
16. T. Saju, M. Velu, Review on welding and fracture of nickel based superalloys, Mater. Today Proc. 46 (17) (2021) 7161 – 7169.
17. B. Mondal, M. Gao, T. A. Palmer, T. DebRoy, Solidification cracking of a nickel alloy during high-power keyhole mode laser welding, J. Mater. Process. Technol. 305 (2022) 117576.
18. K. Łyczkowska, J. Adamiec, The phenomena and criteria determining the cracking susceptibility of repair padding welds of the Inconel 713C nickel alloy, Materials 15 (2) (2022) 634.
19. N. Yue, L. Pei, P. Xu, Z. Jiang, T. Lin, L. Zhou, Y. Liang, Porosity suppression of nickel-based superalloy by modulated base temperature in laser welding and mechanism analysis, J. Mater. Res. Technol. 30 (2024) 4725 – 4738.
20. F. Yan, C. Wang, Y. Wang, X. Hu, T. Wang, J. Li, G. Li, A study of the mechanism of laser welding defects in low thermal expansion superalloy GH909, Mater. Charact. 78 (2013) 21 – 30.
21. S. Wen, Z. Liu, C. Jiang, B. Li, X. Wang, C. Dai, Effect of texture evolution and defect on the crack initiation of a Ni-based superalloy electron beam welded joint, Fatigue Fract. Eng. Mater. Struct. 46 (12) (2023) 4578 – 4590.
22. H. Cheng, L. Kang, J. Pang, B. Xue, D. Du, B. Chang, Effect of the welding position on weld quality when laser welding Inconel 617 Ni-based superalloy, Opt. Laser Technol. 139 (2021) 106962.
23. D. Kojundžić, N. Krnić, I. Samardžić, Weldability of nickel and nickel-based alloys, 3rd International Conference on Materials: corrosion, heat treatment, materials testing and tribology (MTECH 2021) (2021) 214 – 233.
24. B. Arulmurugan, M. Agilan, S. Jerome, M. Arivarasu, M. Manikandan, A. Srikanth, N. Arivazhagan, Investigation of metallurgical and mechanical properties of 21st century nickel-based superalloy 686 by electron beam welding technique, Sādhanā 43 (117) (2018) 1 – 10.
25. K. Han, H. Wang, L. Shen, B. Zhang, Analysis of cracks in the electron beam welded joint of K465 nickel-base superalloy, Vacuum. 157 (2018) 21 – 30.
26. J. Peng, R. Wu, J. Zhang, H. Cai, High-temperature mechanical properties and microstructure of welded joint in GH4169/IC10 dissimilar nickel-based superalloys by vacuum electron beam welding, Mater. Sci. Eng. A. 884 (2023) 145561.
27. A. V. Lyushinsky, Y. V. Nikolich, A. A. Zhloba, S. V. Kharkovsky, A. V. Borovsky, D. S. Karyaka, Diffusion

welding of nickel-based creep-resisting alloys, Weld. Int. 29 (5) (2015) 394 – 396.

28. T. Wu, C. Wang, J. Yang, R. Xu, X. Xue, M. Fu, Y. Zhao, J. Xu, Q. Zhang, P. Lin, X. Yue, T. Lin, P. He, Low temperature and rapid diffusion bonding of Ni_3Al-based superalloy with Ni-based superalloy by spark plasma sintering, J. Mater. Process. Technol. 326 (2024) 118324.
29. D.K. Rajak, D.D. Pagar, P.L. Menezes, A. Eyvazian, Friction-based welding processes: friction welding and friction stir welding, J. Adhes. Sci. Technol. 34 (24) (2020) 2613 – 2637.
30. S. Kumar, A. Mahajan, S. Kumar, H. Singh, Friction stir welding: Types, merits & demerits, applications, process variables & effect of tool pin profile, Mater. Today Proc. 56 (2022) 3051 – 3057.
31. W. Cai, G. Daehn, A. Vivek, J. Li, H. Khan, R.S. Mishra, M. Komarasamy, A state-of-the-art review on solid-state metal joining, J. Manuf. Sci. Eng. 141 (3) (2019) 031012.
32. E. V. Galieva, E. Yu. Klassman, V. A. Valitov, I. I. Musabirov, Pressure welding of heat-resistant EK61 and EP975 nickel-based superalloys at a temperature of 900°C, Lett. Mater. 13 (4) (2023) 347 – 352. DOI: 10.22226/2410-3535-2023-4-347-352 Webpage
33. A.K. Akhunova, V.A. Valitov, E.V. Galieva, Computer simulation of pressure welding of heat resistant heterophase nickel-based superalloys specimens through an interlayer, Lett. Mater. 11 (3) (2021) 254 – 260. (in Russian)
34. R.R. Ye, H.Y. Li, R.G. Ding, T.J. A. Doel, S. Bray, A. Walpole, P. Bowen, Microstructure and microhardness of dissimilar weldment of Ni-based superalloys IN718-IN713LC, Mater. Sci. Eng. A. 774 (2020) 138894.
35. H.S. Kang, M. Gwak, B.J. Kim, K. Park, Y. Son, S.M. Seo, S. Kim, H. Lee, J.G. Kim, Repairing weld for directly solidified Ni-based superalloy substrates using directed energy deposition of Inconel 625, Mater. Sci. Eng. A. 913 (2024) 147083.
36. T. Tang, Q. Shi, J. Zhou, C. Zhang, W. Liang, M. Zhou, G. Zhang, G. Chen, Kissing bond defects in inertia friction welds of IN718 alloys: Experiment and prediction, J. Mater. Process. Technol. 338 (2025) 118786.
37. R.R. Gabbasov, E.V. Galieva, E.Yu. Klassman, V.A. Valitov, Effect of pressure welding temperature on the microstructure and mechanical properties of solid-state joints of wrought nickel-based EK79 and EP975 superalloys, Lett. Mater. 14 (2) (2024) 155 – 160.
38. R. R. Gabbasov, A. A. Tagirova, E. V. Galieva, V. A. Valitov, Formation of solid-state joints of dissimilar alloys based on Ni and Ni_3Al, Lett. Mater. 14 (4) (2024) 475 – 481.
39. S. Lister, O. L. Blanch, D. S. Fernandez, J. Pope, G. J. Baxter, S. Bray, M. Jackson, A machinability assessment of the novel application of field-assisted sintering technology to diffusion bond (FAST-DB) and functionally grade dissimilar nickel-based superalloys, Metall. Mater. Trans. A. 54 (11) (2023) 4396 – 4408.
40. Z. Zhang, J. Liu, C. Zhu, Y. Huang, X. Wang, Y. Zhou, J. Wang, J. Li, Effects of post-weld heat treatment on microstructure and mechanical properties of the brazed joint of a novel fourth-generation nickel-based single crystal superalloy, Materials. 16 (8) (2023) 3008.
41. Y. Huang, R. Zhang, F. Wang, Z. Zhou, P. Zhang, J. Yan, Y. Yuan, Y. Gu, C. Cui, Y. Zhou, X. Sun, Effect of PWHT on microstructure and mechanical properties of welded joint of a new Fe-Ni-based superalloy, Mater. Sci. Eng. A. 906 (2024) 146699.
42. H. Wang, K. Han, B. Zhang, Effect of post-weld solution treatment on microstructure and mechanical properties of electron beam welded IN738LC joint, J. Mater. Res. Technol. 15 (2021) 3047 – 3059.
43. B.S. Lomberg, S.V. Ovsepyan, M.M. Bakradze, Alloying and heat treatment features of Ni-base superalloys for new jeneration GTE disks, Aviat. Mater. Technol. 2 (15) (2010) 3 – 8.
44. A. A. Ganeev, V. A. Valitov, M. I. Nagimov, V. M. Imayev, Effect of hot forging on the microstructure and superplastic properties of the powder nickel base superalloy EP741NP, Lett. Mater. 10 (1) (2020) 100 – 105. (in Russian)